CrossMark

ORIGINAL PAPER

Voltammetric aptamer based detection of HepG2 tumor cells by using an indium tin oxide electrode array and multifunctional nanoprobes

Duanping Sun[1] · Jing Lu[1] · Xiangyan Wang[1] · Yuanqing Zhang[1] · Zuanguang Chen[1]

Abstract The authors describe a method for the detection and determination of human liver cancer cells in blood. The cytosensing system consists of a microfabricated chip-based electrochemical aptasensor that contains multifunctional hybrid electrochemical nanoprobes and an indium tin oxide (ITO) electrode array interface functionalized with cell-targeting aptamer and gold nanoparticles (AuNPs). The thiolated cell targeting aptamer (referred to as TLS11a) was immobilized on the ITO electrode/AuNPs for specific adhesion of hepatocellular carcinoma cells (HepG2). The hybrid nanoprobe system consists of hydroquinone (HQ) as an electrochemical probe, horseradish peroxidase (HRP), and an aptamer/hemin/G-quadruplex aggregate that was immobilized on gold/palladium-functionalized ZnO nanorods (ZnO@Au-Pd). The nanoprobes are capable of amplifying the voltammetric signal and capturing the target cells. Best operated at around −90 mV (vs Ag/AgCl), the electrode has a linear response that covers the 10^2 to 10^7 HepG2 cells per mL concentration range, with a 10 cell per mL detection limit. Captured cells may be released from the electrode via electrochemical desorption to break the Au-S bonds.

Duanping Sun and Jing Lu contribute equally to this paper.

✉ Yuanqing Zhang
   zhangyq65@mail.sysu.edu.cn

✉ Zuanguang Chen
   chenzg@mail.sysu.edu.cn

1   School of Pharmaceutical Sciences, Sun Yat-Sen University, Guangzhou 510006, China

Introduction

Liver cancer is the third most deadly cancer worldwide [1, 2]. α-Fetoprotein (AFP) is often used as a biomarker for screening and diagnosing primary liver cancer [3, 4]. However, AFP is not always reliable as a liver cancer biomarker because the serum level of AFP may be higher in many other liver diseases. For monitoring liver cancers, it is not convincing for detecting the blood level of AFP in the clinical study. Therefore, the sensitive and specific analysis of liver cancer cells has considerable clinical significance in cancer diagnosis.

Considering the important role of tumor cells in cancer diagnosis and management, developing highly sensitive and selective biosensors has become a hot research topic. Various approaches, including surface plasmon resonance [5], microcantilever [6], electrochemiluminescence [7, 8] and electrochemistry have been applied for cancer cells analysis [9]. However, the selectivity and sensitivity of these methods is still not high enough for clinical sample analysis. Compared with other methods, electrochemical aptasensors have attracted considerable attention in the analysis of cancer cells because of its advantages such as rapid response, high selectivity and satisfied sensitivity [10, 11]. Aptamer is the artificial single-stranded nucleic acid sequence that can specifically bind to target molecules, proteins and entire cells by the formation of three-dimensional structures [12]. For example, TLS11a aptamer has been identified to specifically recognize human hepatocellular carcinoma HepG2 cells via the

specific binding to the membrane surface of liver cancer cells [13, 14]. Various electrochemical aptamer cytosensors for cancer cells have been performed. For example, Zhu's group fabricated a series of multifunctional electrochemical nanoprobes for signal amplification toward electrochemical cytosensing [15–17]. Peng's group took advantage of a dual-aptamer recognition method for selective and sensitive electrochemical analysis of cancer cells [18]. Wang's group used layer-by-layer technology to develop an electrochemical cytosensing platform for detecting HeLa cancer cells [19]. Our group fabricated electrochemical aptamer cytosensors for selective and sensitive detection of HepG2 cells by using TLS11a aptamer [20, 21]. Although these electrochemical cytosensors exhibited selectivity and sensitivity for detection of cancer cells, it is still necessary to design a portable and disposable tool with high specificity and sensitivity for clinical sample analysis.

Microchip, or lab on a chip, are now widely considered as an enabling technology in cancer cell biology because they possess a variety of advantages, including multiplexing ability, low reagent consumption and potential for integration. In particular, microchip-based electrochemical platforms have progressed rapidly for cancer cell detection because of their ease of miniaturization and automation [22–24]. Zhu's group designed an integrated microfluidic electrochemical system for the dynamic evaluation of glycan expressions on cancer cell surface [25]. Kelley's group fabricated a nanoparticle labeling-based cytosensor for highly specific electrochemical analysis of circulating tumor cells [26]. Yu's group did a lot of work for sensitive electrochemical detection of cancer cells by developing lab-on-paper techniques [27–31]. Indium tin oxide (ITO), an inexpensive electrochemical material with stable electrochemical properties and high electrical conductivity, can be integrated on a microfabricated chip by using etching technologies [32]. These advantages makes the chip integrated with ITO electrode arrays, the aptamer technique and electrochemical methods for detection of human liver cancer cells.

This paper describes an electrochemical cytosensor array for highly specific and sensitive detection of human liver cancer cell. Compared with our previous work [20, 21], the cytosensor array was prepared by using gold nanoparticles (AuNPs) and TLS11a aptamer to modify working electrodes of screen-printed ITO electrodes for recognizing and capturing target HepG2 cells. And the hybrid nanoprobes of horseradish peroxidase (HRP), TLS11a aptamer, hemin/G-quadruplex HRP-mimicking DNAzyme, and hydroquinone (HQ) immobilized on the surface of gold/palladium hybrid functionalized ZnO nanorods (ZnO@Au-Pd) were designed to amplify the electrochemical detection signal and improve the selectivity of the target cancer cells. The high detection sensitivity and selectivity are achieved by assembling aptamer-functionalized AuNPs nanostructures on ITO electrode array surface and utilizing hybrid nanoprobes with nanomaterials, redox tags, cell-targeting aptamer and signal amplifying enzyme. Moreover, this method was further used for imaging cancer cells in ITO electrodes. After electrochemical detection, the device can release the captured cells by an electrochemical reductive desorption method. This electrochemical cytosensing platform provides a useful tool for cancer cell detection in clinical diagnostics.

Experimental section

Reagents and materials

Sodium hydroxide (NaOH), zinc nitrate hexahydrate ($Zn(NO_3)_2 \cdot 6H_2O$), gold chloride hydrate ($HAuCl_4 \cdot 3H_2O$), potassium tetrachloropalladate (K_2PdCl_4), methanol, sodium citrate, ascorbic acid (AA), hydroquinone (HQ), horseradish peroxidase (HRP) H_2O_2 (30%, w/w) and hemin were purchased from Aladin Chemistry Co., Ltd. (Shanghai, China, http://www.aladdin-e.com). Cell Counting Kit-8 (CCK-8) was obtained from BestBio Biotechnology Co., Ltd. (Shanghai, China, http://www.bestbio.com.cn). 6-mercapto-1-hexanol (MCH) was purchased from J&K Chemical Ltd. (Guangzhou, China, http://www.jkchemical.com). Red cell lysis buffer, the thiolated TLS11a aptamer and signal probe were obtained from Sangon Biotechnology Co., Ltd. (Shanghai, China, http://www.sangon.com), and the sequences were listed in Table S1. The signal probe consists of two strands, a cell-targeted TLS11a aptamer sequence and a G-quadruplex-forming sequence. Sylgard 184 silicone elastomer and curing agent were obtained from Dow Corning (Midland, MI, USA, http://www.dowcorning.com/). Indium tin oxide (ITO)-coated glass (150 nm thick and resistance <15 Ω per square) was purchased from Xiangcheng Technology Co., Ltd. (Shenzhen, China). Phosphate buffered saline (PBS) was prepared with 137 mM NaCl, 2.7 mM KCl, KH_2PO_4 and Na_2HPO_4. The PBS (pH 7.0, 100 mM) was served as a working solution for detection and the PBS (pH 7.4, 10 mM) was utilized as a washing solution. Ultrapure water was obtained from a Milli-Q purification system with the resistivity of 18.2 MΩ cm. Other chemical reagents were of analytical grade and used without further purification.

Apparatus and measurements

Scanning electron microscopy (SEM) images were collected from a thermal field emission scanning electron microscope (FEI Quanta 400, Netherlands, https://www.fei.com/home). Atomic force microscopy (AFM) images were obtained on a Scanning probe microscope (SPM, Dimension FastScan Bio,

Bruker, www.bruker.com/). X-ray photoelectron spectroscopy (XPS) experiments were employed using a Thermo-VG Scientific ESCALAB 250 spectrometer (Thermoelectricity Instruments, USA, https://www.thermofisher.com/cn). The cell images were observed by Nikon Eclipse fluorescence microscope (Nikon Instruments Co., Japan, http://www.nikon.com/). Cyclic voltammetry (CV), differential pulse voltammetry (DPV) and electrochemical impedance spectroscopy (EIS) were carried out using a RST5100F electrochemical workstation (Suzhou Risetest Instrument Co., Ltd., Suzhou, China, http://www.cnrst.com/). A standard three-electrode system, consisting of a Pt auxiliary electrode, an Ag/AgCl reference electrode and a bare or modified ITO (2 mm in diameter) working electrode, was used in all electrochemical measurements.

Cell culture and collection

Human liver hepatocellular carcinoma HepG2 cells, human normal hepatocyte L02 cells and human breast cancer MCF-7 cells were cultured in Dulbecco's modified Eagle's medium (DMEM), supplemented with 10% v/v fetal bovine serum (FBS), and penicillin (100 units mL^{-1})/streptomycin (100 units mL^{-1}) (Gibco Invitrogen Co., MD, USA) in an incubator (37 °C, 5% CO_2). At the logarithmic growth phase, the cells were treated with 0.25 mg mL^{-1} trypsin until they detached and washed with PBS solution twice by centrifugation at 1000 rpm (rcf = 94) for 4 min. Finally, the sediment was dissolved in the PBS solution (10 mM, pH 7.4) to obtain a homogeneous cell suspension.

Blood sample preparation

Fresh blood was collected from healthy volunteers in the First Affiliated Hospital of Sun Yat-Sen University. Different number of HepG2 cells were spiked into the human peripheral blood. After this step, 1 ml of red blood cell lysis buffer were added into blood, and incubated at room temperature for 5 min, then washed thrice with a pH 7.4 PBS buffer. Lastly, the sediment was dissolved in 10 mM pH 7.4 PBS solution to obtain a homogeneous cell suspension.
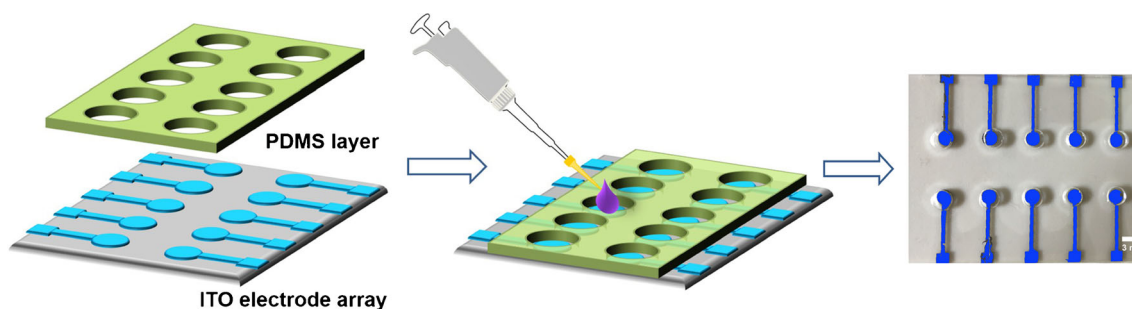
Chip fabrication

The chips with ITO working electrodes were fabricated using combined screen-printing and wet etching in ITO glasses, as shown in Fig. S1. The procedures were referred to a previously reported protocol [33]. First, the electrode image was designed and printed onto a silk-screen. These ITO-coated glasses were carefully cleaned with a detergent solution, followed by sonication for 5 min in ethanol and ultrapure water, respectively. After rinsed with water, the ITO-coated glasses were allowed to dry at room temperature. Then, we brushed the oil ink through the fabricated silk-screen onto the ITO layer. The glass plate was dried for 15 min at 80 °C and etched with prepared solutions (H_2O: HCL: $FeCl_3$ = 1:1:3) for 30 min. After removing the oil ink, the ITO working electrodes were fabricated on the glass substrate (Fig. S2).

The PDMS oligomer and curing agent were mixed in a ratio of 10:1 (w/w) and PDMS chip was cured at 80 °C for 1 h. A blank section of PDMS was punched with a hole and then attached on the ITO electrode array to provide an identical area for electrochemical experiment. The ITO-coated glass substrate and the prepared PDMS chip can be reversibly bonded by simply putting them together (Fig. 1).

Synthesis of ZnO@au-Pd nanocomposites

ZnO@Au-Pd nanocomposites were prepared according to a previously reported method with a modification [34, 35]. Briefly, a aqueous solution of NaOH (4 M, 10 mL) was added to 10 mL of a $Zn(NO_3)_2 \cdot 6H_2O$ (0.5 M) aqueous solution. After sonication for 5 min, the mixture solution was stirred for 12 h. The ZnO nanoflowers products were collected and washed with ethanol and ultrapure water alternately several times and finally dried at 60 °C. After this, 2 mL of $HAuCl_4$ (1% w/w) and 0.5 mL of methanol (99.5% v/v) were added to 10 mL of ultrapure water. The pH value of the mixture was adjusted to 7–8 by 0.01 M NaOH solution. Then, 15 mg of the prepared ZnO was added to the mixture under stirring for about 1 h. The mixture was maintained at 120 °C for 1 h. The obtained ZnO@Au nanocomposites were washed with

Fig. 1 Schematic illustration of the ITO electrode array-based chip for electrochemical cytosensing and photograph of the fabricated chip (The electrodes were colored by blue ink)

ultrapure water and ethanol alternately several times and dried at 60 °C in the air.

The ZnO@Au nanocomposites were heated to a boil and 2 mL of 1% K_2PdCl_4 were added, followed by the addition of 5 mL of 1% AA and 3 mL of 1% sodium citrate, which were used as reductant for the reduction of K_2PdCl_4. After the colloidal suspension was heated for about 30 min, Pd-Au hybrid functionalized ZnO nanorods (ZnO@Au-Pd) was obtained due to the formation of Pd shell driven by the Au seeds acting as nucleation centers [34]. The precipitates were collected by centrifuging, washed with ultrapure water and ethanol alternately several times and finally dried in a vacuum drying oven.
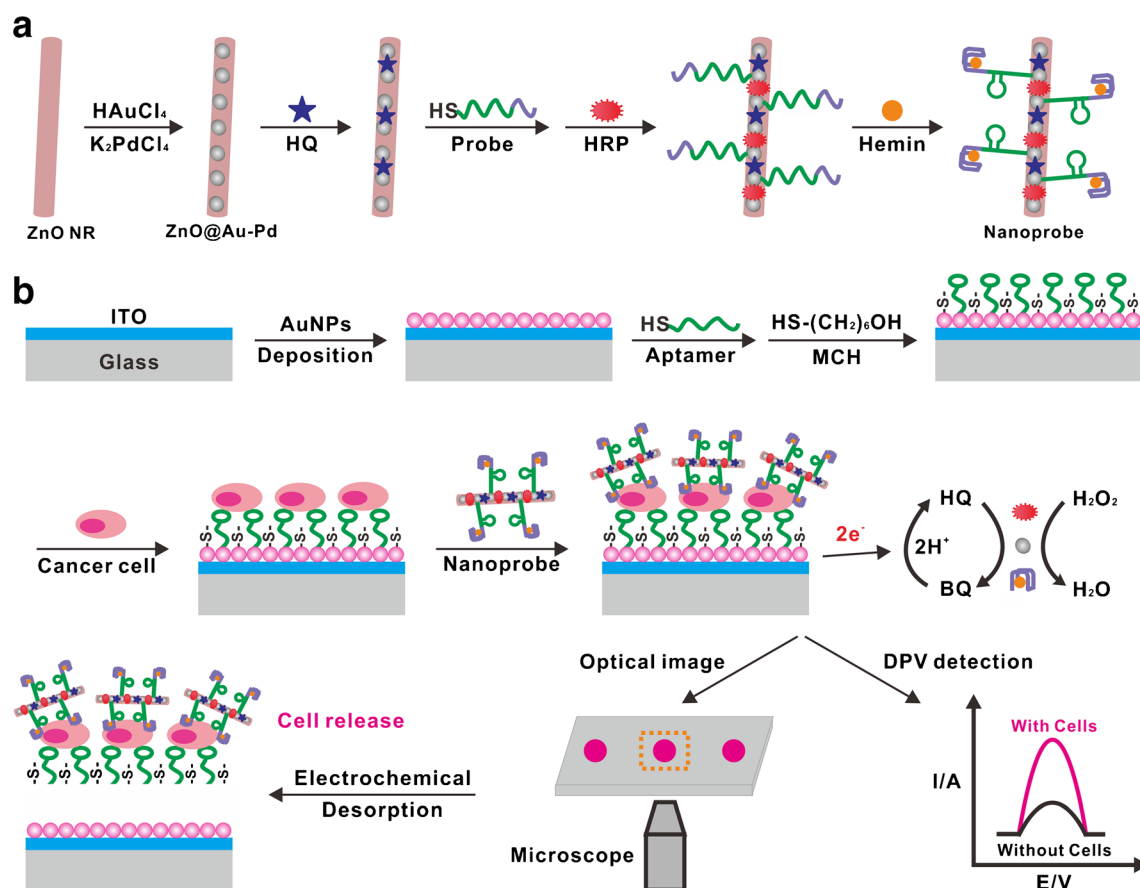
Nanoprobes fabrication

The fabrication procedure of the nanoprobes was illustrated in Fig. 2a. HQ, HRP and DNA probe were immobilized onto the prepared ZnO@Au-Pd nanocomposites according to the following steps: firstly, 1 mL HQ (3 mM) was added into the ZnO@Au-Pd nanocomposites suspension (10 mg in 1 mL PBS) and set on a shaker at room temperature for about 6 h, followed by centrifugation at 11000 rpm (rcf = 11,363) and

washing with ultrapure water. Then, 50 μL of thiolated capture probe (5 μM) and 50 μL of HRP (1 mg mL^{-1}) were added to the solution and the resulting solution was stirred mechanically for 12 h at 4 °C. Subsequently, hemin (0.1 mg) was added into the mixture (pH 7.0) for 2 h at 4 °C, followed by washing with PBS solution. The prepared ZnO@Au-Pd–HQ–HRP–aptamer/hemin/G-quadruplex hybrid nanoprobes were finally resuspended in PBS solution and stored at 4 °C.

Electrochemical measurements

The major steps in the assembly process of the cytosensor was illustrated in Fig. 2b. The ITO electrodes were cleaned sequentially with acetone, ethanol, and ultrapure water and dried at room temperature. Electrodeposition of AuNPs nanostructured ITO electrodes was carried out at the plating potentials of −0.20 V for 20 s in the HAuCl$_4$ solution (w/w 1%). After deposition, the AuNPs/ITO working electrode was rinsed with ultrapure water and allowed to dry at room temperature.

Then, thiolated TLS11a aptamer (5 μM, 10 μL) was immediately applied on the AuNPs-modified ITO electrode surface and incubated at 4 °C for 16 h. The modified ITO electrode was subsequently incubated with 1 mM MCH (50 μL) at

Fig. 2 a Schemes illustrating the processes for the fabrication of ZnO@Au-Pd-HQ-HRP-G-quadruplex/hemin/aptamer hybrid electrochemical nanoprobe. **b** Schemes illustrating the assembly processes in the construction of the electrochemical aptamer cytosensor

room temperature for 1 h to block the remaining active sites and then rinsed with PBS solution thoroughly. Subsequently, 20 μL of the cell suspension with different concentration was dropped onto the modified ITO electrode array and incubated for 1 h at 37 °C to capture the target cells. At last, the cell-captured electrodes was incubated with 10 μL of nanoprobes at 37 °C for 1 h, and washed thoroughly with PBS solution. For electrochemical measurement, the electrode was placed in 0.1 M PBS (pH 7.0) containing 2.0 mM H_2O_2. DPV measurements were performed from −0.3 to 0.2 V (vs. Ag/AgCl) with a pulse amplitude of 50 mV. After that, an electrochemical reductive desorption method was employed to break Au–S bond on the ITO electrode surface to release the captured cancer cells.

Optical imaging

In order to visualize the cell viability, the captured HepG2 cells were stained after incubation with nanoprobes by a cell viability indicator of calcein-AM (5 μM) at 37 °C for 15 min and thoroughly rinsed with PBS. Lastly, the ITO chip was placed in a commercial cell culture dish for imaging cells.

Results and discussion

### Design and characterization of multifunctional nanoprobes

For electrochemical cytosensing, we can improve the detection sensitivity by using electrochemical nanoprobes for signal amplification. In the present work, the nanoprobes were fabricated via a layer-by-layer assembly method (Fig. 2a). The ZnO nanorod arrays, with high electron mobility and a large surface-to-volume ratio, are used to be a promising nanocarriers. The Au-Pd nanomaterials have good stability and conductivity, a high surface area and natural peroxidases-mimicking ability. Therefore, ZnO@Au-Pd nanocomposites are performed as the nanocarriers to load biomolecules, for example redox-tags, aptamer and natural peroxidases.

The hybrid nanoprobes are multifunctional, capable of specific cell targeting and multivalent signal amplification. HQ, a common electroactive mediator, is used as redox-tags for generating the electrochemical signals in designed nanoprobes. We integrated the G-quadruplex-forming sequences and TLS11a aptamer sequences into one single-stranded DNA probe. The cell-targeting TLS11a aptamer have been identified for the recognizing HepG2 cells. And the hemin/G-quadruplex DNAzymes, formed by intercalating hemin into the guanine-rich DNA probe, has been widely used as HRP-mimicking DNAzyme electrocatalysts for electrochemical sensing. The thiolated DNA probe can be conjugated to the ZnO@Au-Pd nanocomposites through metal-thiol interactions. The hemin/G-quadruplex DNAzymes and HRP immobilized on the nanomaterials dramatically amplifies the electrochemical signals due to the Au@Pd nanoparticles, hemin/G-quadruplex DNAzymes and HRP catalyzed oxidation of the redox-tags with H_2O_2.

SEM was used for demonstrating the morphologies of the synthesized ZnO nanorod and ZnO@Au-Pd nanocomposites. The ZnO nanorod was mainly composed of flower-like hierarchical structures and the nanorod had a smooth surface (Fig. 3a). After $HAuCl_4$ and K_2PdCl_4 was added, as seen from Fig. 3b and c, some nanoparticles were observed on the surface of ZnO nanoflowers, indicating that the gold-palladium hybrid functionalized ZnO nanoflowers were successfully fabricated.

The chemical composition of the fabricated ZnO@Au-Pd nanocomposites were further characterized by XPS measurements. As shown in Fig. S3A, the XPS fully scanned spectra demonstrated the existence of characteristic elements of gold, palladium and zinc in nanomaterials. The Au 4f doublet (83.79 and 87.5 eV; Fig. S3B), the Pd 3d doublet (335.65 and 340.95 eV; Fig. S3C), and Zn 2p doublet (1021.49 and 1044.6 eV; Fig. S3D) firmly confirmed the accomplishment of ZnO@Au-Pd nanocomposites. CCK-8 assays were performed to evaluate the cytotoxicity of the ZnO@Au-Pd nanocomposites for HepG2 cells at various concentrations (Fig. S4). The results show that the viabilities of HepG2 are not significantly different compared to that for the controls and the ZnO@Au-Pd nanomaterials are suitable to be the sensing nanocarriers.


Fig. 3 SEM images of a ZnO and b and c ZnO@Au-Pd at different magnifications
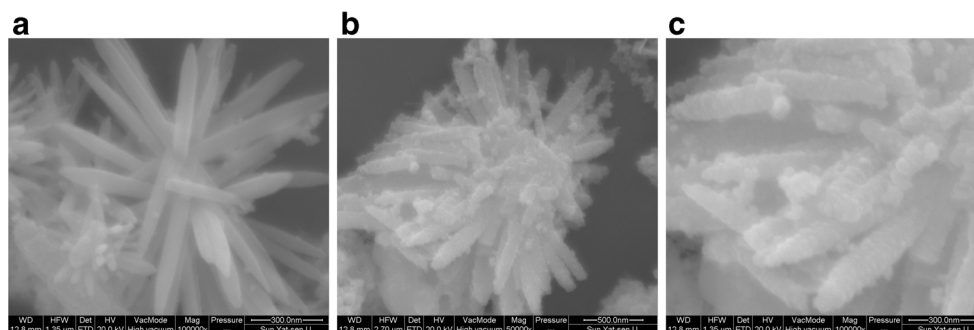
Characterization of the cytosensor

To characterize the stepwise cytosensor assembly process, CV, SEM, AFM and EIS measurements were used to record the behavior of the cytosensor. Electrodeposition time of nanostructured electrode was a significant parameter for the electrochemical cytosensing platform. Fig. 4a shows the CV curves of the bare ITO electrode and different electrodepositing times of AuNPs modified ITO electrode. AuNPs modified ITO electrode had large peak currents (curve b, c and d) compared with the bare ITO electrode (curve a). With the increase of the electrodepositing time from 10 to 30 s, the CV current response increased accordingly. And the peak current started to plateau after 20 s. The result might be ascribed to the fact that a long electrodepositing time resulted in the formation of multilayered AuNPs films on the ITO electrode, which was not conducive to electronics transfer [35]. Thus, 20 s was chosen as the optimized electrodepositing time for the cytosensor. Then, we further investigated the stability of the ITO electrode/AuNPs by using a CV experiment. As shown in Fig. 4b, there is almost no change for the current response after continuous scanning 20 circles, implying that the stability of the electrodeposited AuNPs modified ITO electrode is acceptable. SEM and AFM was also utilized to demonstrate the results. Fig. S5 shows a low-magnification SEM image of the AuNPs modified ITO electrode. The glass surface was not modified by AuNPs. Fig. 4c is the enlarged SEM image, we clearly see that AuNPs modified ITO electrode zone maintained good nanostructure. From the AFM image of AuNPs/ITO in Fig. 4d, we can see that the modified electrode surface
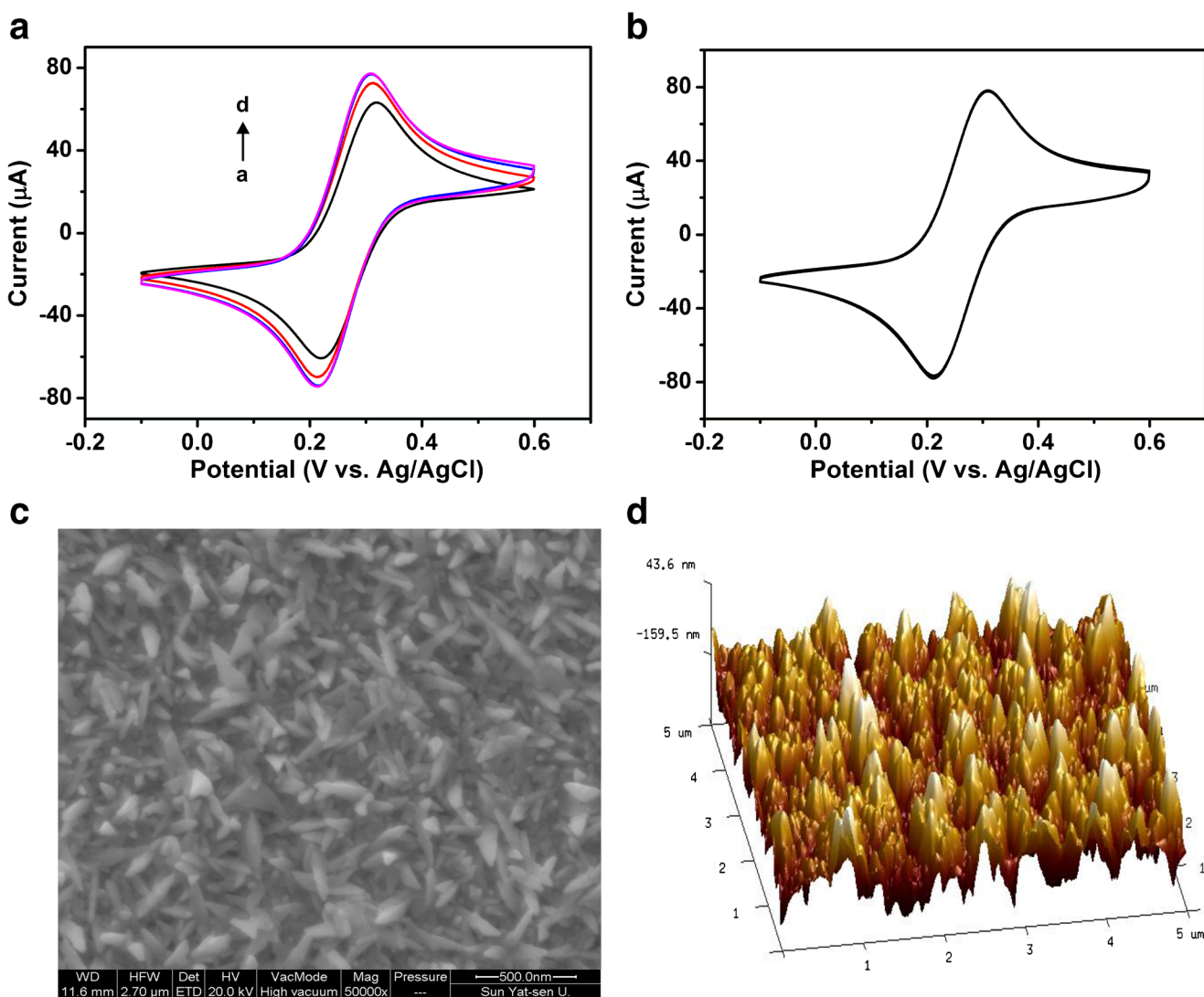
Fig. 4 **a** Cyclic voltammetry responses of (*a*) original ITO electrode and AuNPs modified ITO electrode. The electrolyte solution is 0.5 M KCl containing 5 mM $[Fe(CN)_6]^{4-/3-}$. The scan rate is 100 mV s^{-1}. The electrodes of (*b*), (*c*), and (*d*) are obtained by electrodeposition in HAuCl$_4$ solution for 10, 20, and 30 s, respectively. **b** Stability of the ITO electrode/AuNPs under successive CV scans for 20 cycles. **c** SEM image and **d** AFM image of AuNPs modified ITO electrode
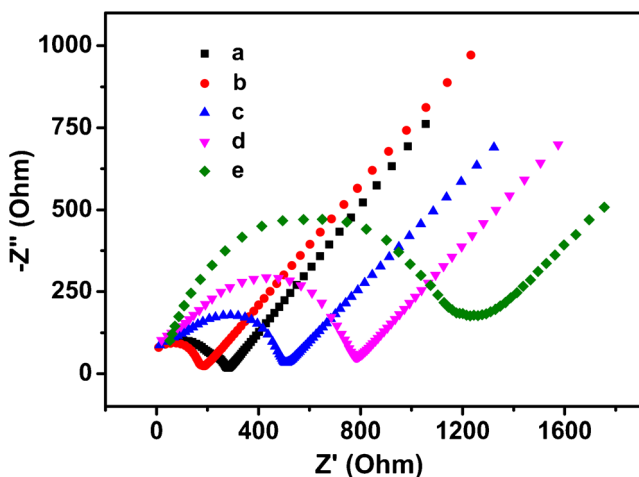
Fig. 5 Electrochemical impedance spectra of **a** bare ITO electrode, **b** ITO electrode/AuNPs, **c** ITO electrode/AuNPs/TLS11a aptamer, **d** ITO electrode/AuNPs/TLS11a aptamer/MCH, and **e** ITO electrode/AuNPs/ TLS11a aptamer/MCH/HepG2 cell. The electrolyte solution is 0.5 M KCl containing 5 mM $[Fe(CN)_6]^{4-/3-}$. The amplitude is 10 mV and the impedance spectral frequency is $0.1\text{-}10^5$ Hz

bare ITO electrode, a small semicircle portion was observed (curve a), indicating the good electron-transfer capability. After the electrodeposition of AuNPs on ITO electrode, the semicircle diameter became smaller (curve b) compared with the bare ITO electrode. The AuNPs films can not only increase the electrode surface for aptamer immobilization, but also enhance the electrical conductivity of the ITO electrode. Then after thiolated TLS11a aptamer was attached to the AuNPs/ITO electrode surface through Au-S bond, the electron transfer resistance increased significantly (curve c), suggesting that aptamer molecules blocked the electron exchange between the AuNPs/ITO electrode layer and redox probe $[Fe(CN)_6]^{3-/4-}$. After blocking with MCH, we observed an increase in diameter of the semicircle (curve d). Moreover, the adhesion of cancer cells on the electrode interface leaded the obvious increase of the resistance (curve e). The results have confirmed the successful fabricated process of the cytosensor.

Optimization of the experimental conditions

After the cancer cells were captured, the electrodes were incubated with the fabricated nanoprobes to form an aptamer-cell-nanoprobe sandwich-type platform. The nanoprobes were used to improve the sensitivity of the cytosensor. The optimum conditions (the amount of nanoprobe solution, HepG2 cells incubation time and the concentration of H_2O_2) were

owns a relatively high roughness and increases the effective surface of ITO electrode, which is consistent with the SEM results.

EIS is a facile and powerful method to monitor the layer-by-layer assembly processes. Fig. 5 displays the EIS (Nyquist plots) of the ITO electrode modification layer by layer. The semicircle diameter of the Nyquist plots is closely linked with the charge-transfer resistance at the electrode interface. For the

Fig. 6 **a** Differential pulse voltammetry responses of the cytosensor for different HepG2 cell concentrations (from curve a to f: 1×10^2, 1×10^3, 1×10^4, 1×10^5, 1×10^6 and 1×10^7 cells mL^{-1}). The inset shows the calibration curve of the linear response for HepG2 cells. **b** Specificity investigations of the cytosensor for different types of cells. The concentration of cells was 10^5 cells mL^{-1} except for the blank control. **c-d** Fluorescence microscopy images of calcein-AM-stained HepG2 cells at different concentrations captured on the MCH/aptamer/AuNPs/ ITO electrode after incubation with nanoprobes for 1 h
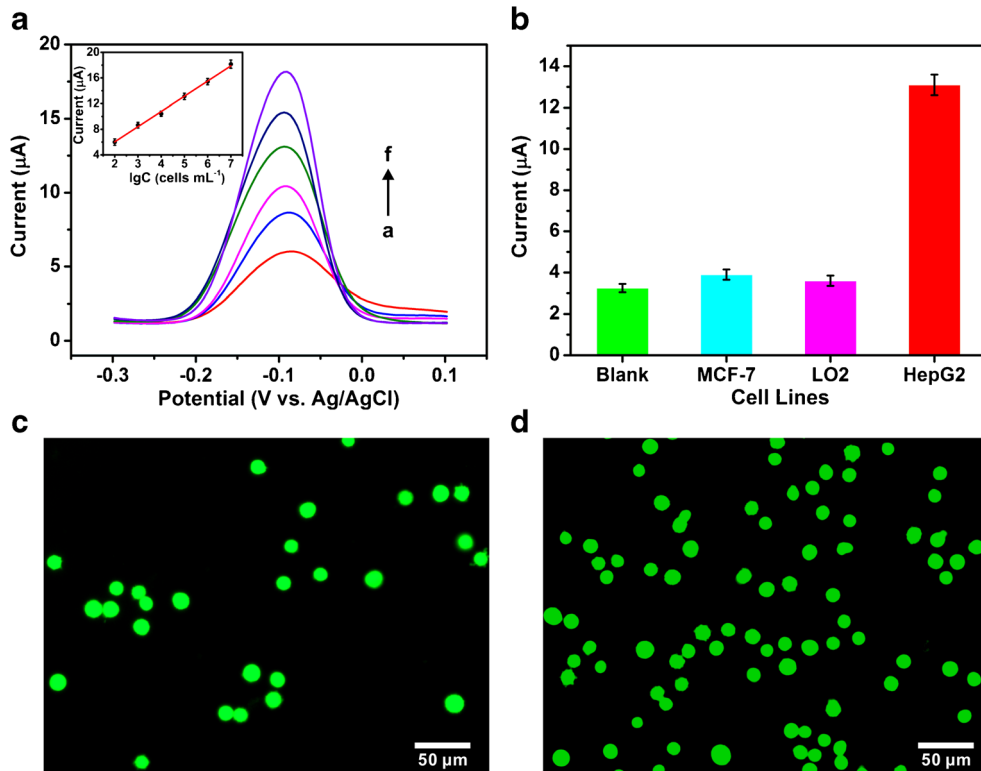
Table 1 Comparison of this ITO electrode array-based electrochemical cytosensor with other reported cytosensors for HepG2 cell detection

Cytosensor type	Analytical method	Linear range (cells mL^{-1})	Detection limit (cells mL^{-1})	Reference
Microcantilever aptasensor	Microcantilever assay	1×10^3 to 1×10^5	300	[6]
Electrochemiluminescent immunosensor	Electrochemiluminescence	3×10^2 to 1×10^4	256	[7]
Electrochemical aptasensor	Impedance spectroscopy	1×10^2 to 1×10^6	2	[14]
Electrochemical aptasensor	Differential pulse voltammetry	1×10^2 to 1×10^7	15	[21]
Electrochemical aptasensor	Differential pulse voltammetry	1×10^2 to 1×10^7	10	This work

measured, as shown in Fig. S6. A detailed description can be found in the Supplementary information.

## Electrochemical detection of HepG2 cells

High sensitivity and selectivity plays a significant role in the analysis of cancer cells. Under the optimized conditions, the DPV responses for different concentrations of HepG2 cells are shown in Fig. 6a. DPV current signals increase obviously with the increasing concentration of HepG2 cells. Best operated at around −90 mV (vs Ag/AgCl), the DPV currents are linearly dependent on the logarithm values of number of HepG2 cells ranging from 1×10^2 to 1×10^7 cells mL^{-1}. The linear regression equation is I (μA) =1.3022 + 2.3682 lgC$_{cells}$ (cells mL^{-1}) with a correlation coefficient of 0.9959 (n = 3). And the detection limit for HepG2 cells is determined to be 10 cells mL^{-1} using 3σ/k (σ is the standard deviation of the blank measures and k is the slope of the corresponding calibration curve). The high detection sensitivity may be a consequence of the synergistic effects of excellent conductivity of AuNPs/ITO, the loading of a large amount of redox-tags in ZnO@Au-Pd and the high catalytic activity of HRP and hemin/G-quadruplex DNAzymes. The multifunctional nanoprobes dramatically amplify the electrochemical signals due to the Au-Pd nanoparticles, hemin/G-quadruplex DNAzymes and HRP catalyzed oxidation of the redox-tags (HQ) with H_2O_2. The performance of the electrochemical cytosensor was better than those of reported cytosensors, such as microcantilever aptasensor and electrochemiluminescence cytosensor (Table 1).

For investigating the selectivity of the cytosensor toward HepG2 cells, different types of cells, such as MCF-7 and L02 cells were tested. As shown in Fig. 6b, compared with the blank control, electrochemical signal change of the cytosensor shows a negligible change for the MCF-7 cells and L02 cells. In addition, cell culture medium and HepG2 cell lysates also show a small current response (Fig. S7). Based on above results, this cytosensor had good selectivity for the detection of HepG2 cells. To visualize the cell viability, the captured HepG2 cells were stained after incubation with nanoprobes by a cell viability indicator of calcein-AM. The fluorescence signals show that the HepG2 cells are alive during the electrochemical cytosensing processes (Fig. 6c and d).

To evaluate the repeatability of our protocol, the precision of the cytosensor was measured for three replicate measurements. When the cell concentrations of HepG2 were 10^5 cells per mL, the electrochemical cytosensor performed a relative standard deviation of 3.8%, demonstrating the acceptable repeatability of the cytosensor. This electrochemical cytosensor shows good performance in detection and analysis of HepG2 cells with a lower detection limit, a broad linear range, acceptable repeatability and selectivity.

To investigate the feasibility of the cytosensor in blood sample, various amounts of HepG2 (10^2, 10^4 and 10^6 cell mL^{-1}) was spiked into the human blood sample and detected. As shown in Table S2, the recoveries are between 82.3% and 90.4% from 10^2 to 10^6 cells mL^{-1}, indicating the good analytical performance of the method. These results demonstrate that the ITO electrode array-based electrochemical method

Fig. 7 Electrochemical impedance spectra (**a**) and cyclic voltammograms (**b**) of original ITO electrode/AuNPs (*a*) and the regenerated ITO electrode/AuNPs (*b*). The electrolyte solution is 0.5 M KCl containing 5 mM [Fe(CN)$_6$]$^{4-/3-}$. The amplitude is 10 mV and the impedance spectral frequency is 0.1-10^5 Hz. The scan rate is 100 mV s^{-1}
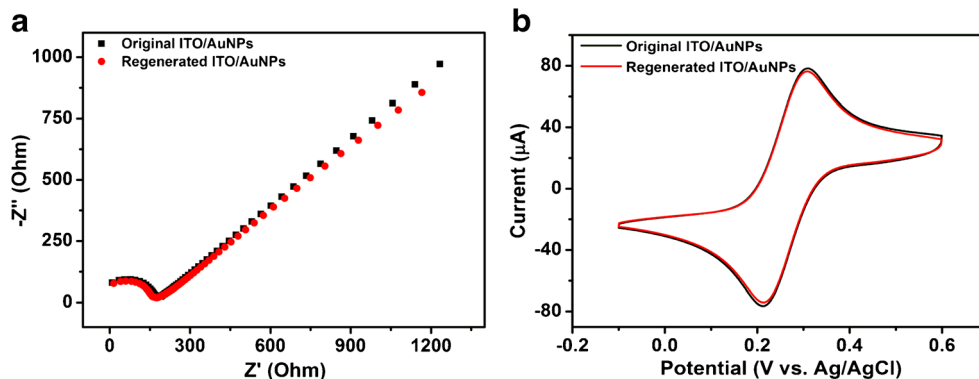
provides a potential clinic diagnostic tool to detect tumor cells in peripheral blood.

Release of captured HepG2 cells

In cancer research, capture, release and culture of cancer cells can promote the progress of anti-tumor therapies. Releasing of captured liver cancer cells was another advantage of the electrochemical cytosensing platform. To realize the release of cancer cells, we performed an electrochemical desorption method to break Au-S interactions and remove captured cells on the electrode. CV and EIS were employed to demonstrate the release of captured cancer cells from the electrode surface. Fig. 7 shows the EIS and CV curves of the original ITO electrode/AuNPs (curve a) and regenerated ITO electrode/AuNPs after electrochemical desorption (curve b). The regenerated AuNPs/ITO electrode has the same peak current and impedance spectra, compared with the original AuNPs/ITO electrode. These results have confirmed that we have successfully fabricated an effective electro-controlled cancer cell capture and release platform by electrochemical methods.

Conclusions

In conclusion, an ITO electrode array-based electrochemical cytosensing platform was successfully constructed for detecting human liver cancer cells in a highly selective and sensitive manner. Compared to the conventional electrochemical methods and our previous work [20, 21], the ITO electrode array-based electrochemical strategy requires small amount of sample and is cost-effective. Best operated at around −90 mV (vs Ag/AgCl), the fabricated super-sandwich cytosensor exhibited a wide linear response ranging from 10^2 to 10^7 cells per mL and a low detection limit of 10 cells per mL for HepG2 cells. Other important advantages are exhibited in which it can capture, detect, image target tumor cells and release the captured cells by the electrochemical reductive desorption method. It also has been successfully applied in detecting HepG2 cell in blood samples. This electrochemical cytosensor have great potential for tumor cell analysis in early diagnostics and therapeutic monitoring of cancers. However, the cytosensor has complicated fabrication processes which may results in poor reliability and future studies must focus on developing a simple, low-cost and integrated platform for clinical application.

References

1. Siegel RL, Miller KD, Jemal A (2015) Cancer statistics, 2015. Ca-Cancer J Clin 65:5–29
2. Siegel RL, Miller KD, Jemal A (2016) Cancer statistics, 2016. Ca-Cancer J Clin 66:7–30
3. Yang JD, Roberts LR (2010) Hepatocellular carcinoma: a global view. Nat Rev Gastroenterol Hepatol 7:448–458
4. Shan J, Ma ZF (2017) A review on amperometric immunoassays for tumor markers based on the use of hybrid materials consisting of conducting polymers and noble metal nanomaterials. Microchim Acta 184:969–979
5. Jia SS, Li PF, Koh K, Chen HX (2016) A cytosensor based on NiO nanoparticle-enhanced surface plasmon resonance for detection of the breast cancer cell line MCF-7. Microchim Acta 183:683–688
6. Chen XJ, Pan YG, Liu HQ, Bai XJ, Wang N, Zhang BL (2016) Label-free detection of liver cancer cells by aptamer-based microcantilever biosensor. Biosens Bioelectron 79:353–358
7. Liu DQ, Wang L, Ma SH, Jiang ZH, Yang B, Han XJ, Liu SQ (2015) A novel electrochemiluminescent immunosensor based on CdS-coated ZnO nanorod arrays for HepG2 cell detection. Nanoscale 7:3627–3633
8. Wang YZ, Hao N, Feng QM, Shi HW, Xu JJ, Chen HY (2016) A ratiometric electrochemiluminescence detection for cancer cells using g-C3N4 nanosheets and ag–PAMAM–luminol nanocomposites. Biosens Bioelectron 77:76–82
9. Hasanzadeh M, Shadjou N, de la Guardia M (2015) Recent advances in nanostructures and nanocrystals as signal-amplification elements in electrochemical cytosensing. Trac-Trend Anal Chem 72:123–140
10. Sheng QL, Cheng N, Bai WS, Zheng JB (2015) Ultrasensitive electrochemical detection of breast cancer cells based on DNA-rolling-circle-amplification-directed enzyme-catalyzed polymerization. Chem Commun 51:2114–2117
11. Shen HW, Yang J, Chen ZP, Chen XP, Wang L, Hu J, Ji FH, Xie GM, Feng WL (2016) A novel label-free and reusable electrochemical cytosensor for highly sensitive detection and specific collection of CTCs. Biosens Bioelectron 81:495–502
12. Ireson CR, Kelland LR (2006) Discovery and development of anticancer aptamers. Mol Cancer Ther 5:2957–2962
13. Shangguan DH, Meng L, Cao ZHC, Xiao ZY, Fang XH, Li Y, Cardona D, Witek RP, Liu C, Tan WH (2008) Identification of liver cancer-specific aptamers using whole live cells. Anal Chem 80:721–728
14. Kashefi-Kheyrabadi L, Mehrgardi MA, Wiechec E, Turner APF, Tiwari A (2014) Ultrasensitive detection of human liver hepatocellular carcinoma cells using a label-free aptasensor. Anal Chem 86:4956–4960
15. Zheng TT, Fu JJ, Hu LH, Qiu F, Hu MJ, Zhu JJ, Hua ZC, Wang H (2013) Nanoarchitectured electrochemical cytosensors for selective detection of leukemia cells and quantitative evaluation of death receptor expression on cell surfaces. Anal Chem 85:5609–5616
16. Zheng TT, Tan TT, Zhang QF, Fu JJ, Wu JJ, Zhang K, Zhu JJ, Wang H (2013) Multiplex acute leukemia cytosensing using multifunctional hybrid electrochemical nanoprobes at a hierarchically nanoarchitectured electrode interface. Nanoscale 5:10360–10368
17. Zheng TT, Zhang QF, Feng S, Zhu JJ, Wang Q, Wang H (2014) Robust nonenzymatic hybrid nanoelectrocatalysts for signal amplification toward ultrasensitive electrochemical cytosensing. J Am Chem Soc 136:2288–2291

18. Qu LM, Xu JH, Tan XF, Liu Z, Xu LG, Peng R (2014) Dual-aptamer modification generates a unique interface for highly sensitive and specific electrochemical detection of tumor cells. ACS Appl Mater Interfaces 6:7309–7315

19. Wang TS, Liu JY, Gu XX, Li D, Wang J, Wang EK (2015) Label-free electrochemical aptasensor constructed by layer-by-layer technology for sensitive and selective detection of cancer cells. Anal Chim Acta 882:32–37

20. Sun DP, Lu J, Chen ZG, Yu YY, Mo MN (2015) A repeatable assembling and disassembling electrochemical aptamer cytosensor for ultrasensitive and highly selective detection of human liver cancer cells. Anal Chim Acta 885:166–173

21. Sun DP, Lu J, Zhong YW, Yu YY, Wang Y, Zhang BB, Chen ZG (2016) Sensitive electrochemical aptamer cytosensor for highly specific detection of cancer cells based on the hybrid nanoelectrocatalysts and enzyme for signal amplification. Biosens Bioelectron 75:301–307

22. Jia XF, Dong SJ, Wang EK (2016) Engineering the bioelectrochemical interface using functional nanomaterials and microchip technique toward sensitive and portable electrochemical biosensors. Biosens Bioelectron 76:80–90

23. Cao JT, Zhu YD, Rana RK, Zhu JJ (2014) Microfluidic chip integrated with flexible PDMS-based electrochemical cytosensor for dynamic analysis of drug-induced apoptosis on HeLa cells. Biosens Bioelectron 51:97–102

24. Li N, Xiao TY, Zhang ZT, He RX, Wen D, Cao YP, Zhang WY, Chen Y (2015) A 3D graphene oxide microchip and a au-enwrapped silica nanocomposite-based supersandwich cytosensor toward capture and analysis of circulating tumor cells. Nanoscale 7: 16354–16360

25. Cao JT, Hao XY, Zhu YD, Sun K, Zhu JJ (2012) Microfluidic platform for the evaluation of multi-glycan expressions on living cells using electrochemical impedance spectroscopy and optical microscope. Anal Chem 84:6775–6782

26. Wan Y, Zhou YG, Poudineh M, Safaei TS, Mohamadi RM, Sargent EH, Kelley SO (2014) Highly specific electrochemical analysis of cancer cells using multi-nanoparticle labeling. Angew Chem Int Ed 53:13145–13149

27. Su M, Ge L, Ge SG, Li NQ, Yu JH, Yan M, Huang JD (2014) Paper-based electrochemical cyto-device for sensitive detection of cancer cells and in situ anticancer drug screening. Anal Chim Acta 847:1–9

28. Wu LD, Ma C, Ge L, Kong QK, Yan M, Ge SG, Yu JH (2015) Paper-based electrochemiluminescence origami cyto-device for multiple cancer cells detection using porous AuPd alloy as catalytically promoted nanolabels. Biosens Bioelectron 63:450–457

29. Su M, Ge L, Kong QK, Zheng XX, Ge SG, Li NQ, Yu JH, Yan M (2015) Cyto-sensing in electrochemical lab-on-paper cyto-device for in-situ evaluation of multi-glycan expressions on cancer cells. Biosens Bioelectron 63:232–239

30. Wu LD, Zhang Y, Wang YH, Ge SG, Liu HY, Yan M, Yu JH (2016) A paper-based electrochemiluminescence electrode as an aptamer-based cytosensor using PtNi@carbon dots as nanolabels for detection of cancer cells and for in-situ screening of anticancer drugs. Microchim Acta 183:1873–1880

31. Liang LL, Su M, Li L, Lan FF, Yang GX, Ge SG, Yu JH, Song XR (2016) Aptamer-based fluorescent and visual biosensor for multiplexed monitoring of cancer cells in microfluidic paper-based analytical devices. Sens Actuators, B: Chem 229:347–354

32. Liu WY, Yang HM, Ge SG, Shen L, Yu JH, Yan M, Huang JD (2015) Application of bimetallic PtPd alloy decorated graphene in peroxydisulfate electrochemiluminescence aptasensor based on ag dendrites decorated indium tin oxide device. Sens Actuators, B: Chem 209:32–39

33. Sun DP, Lu J, Chen ZG (2015) Microfluidic contactless conductivity cytometer for electrical cell sensing and counting. RSC Adv 5: 59306–59313

34. Wang CY, Tan XR, Chen SH, Yuan R, Hu FX, Yuan DH, Xiang Y (2012) Highly-sensitive cholesterol biosensor based on platinum-gold hybrid functionalized ZnO nanorods. Talanta 94:263–270

35. Yang ZH, Zhuo Y, Yuan R, Chai YQ (2015) Amplified thrombin aptasensor based on alkaline phosphatase and hemin/G-quadruplex-catalyzed oxidation of 1-Naphthol. ACS Appl Mater Interfaces 7:10308–10315